

Quick estimation of tsunami induced runup on coastal area

Jing-Hua Lin¹ Chia-Yan Cheng¹ Jin-Li Yu¹ Yang-Yih Chen¹ Guan-Yu Chen²

The main purpose of this study is that extending 1D Carrier-Wu-Yeh algorithm and analytical Green's function (AGF) to estimate the arbitrary irregular waveforms induced runup height and the inundation distance, and further builds a pre-calculated runup dataset. In this study, the multiplication and superposition is employed to replace the direct numerical integration. The waveforms are decomposed as numerous Fourier components using fast Fourier transformation. The corresponding mechanical energy can be calculated beforehand and save the results as a database-form. Using this process, the maximum runup height and the inundation distance can be quick calculated after determining the total mechanical energy. Based on application on the real tsunami events, the comparisons show that the present methodology can shorten the computing time in comparison with the direct numerical integration. Moreover, the present approach also applies on real tsunami events, 2004 Indian tsunami and 2011 Tohoku tsunami, to estimate the runup height and the inundation distance. The forecasted results are quite satisfactory in comparison with the field measurement, and it implies that the reasonable accuracy and the computing efficiency are both considered in this study.

Keywords : 1D Carrier-Wu-Yeh algorithm, analytical Green's function (AGF), 2004 Indian tsunami, 2011 Tohoku tsunami.

1. Introduction

When tsunami waves approach the coastal region from open sea, waves surge up and down along the beach or the sloping seawall/embankment due to the shoaling effect. This vertical motion is called runup and rundown of the tsunami. The maximum wave elevation measured from the stationary water level is called runup height. The phenomenon is completed within several seconds. The runup height is useful for planning refuge areas. The runup height is influenced by the shape of coastlines, the bathymetry, the slope, and the arrangement of existing structures inland. Numerous empirical formulas have been applied to evaluate the runup height; however, these formulas usually have been associated with a particular slope and incident waveform. On the other hand, the inundation range is related to geomorphic factors after the tsunami invades the land, and the flow velocity on land can be approximately evaluated using the runup height. Thus, quickly-early estimating of tsunami-induced runup height beforehand is worth while to study the issue in real tsunami events.

Combining the 2D tsunami model and the high-resolution digital terrain data, the runup height and inundation area can be estimated with good accuracy based on the accurate fault parameters. However, 2-D tsunami simulations are usually taken one hour or more depending on the grid size and computer's capability. Thus, in the viewpoint of prevention and mitigation of tsunami disasters, a real time simulation on the coastal region is not feasible for a near field tsunami. In practice, pre-computed scenarios and their combinations are used by the National Oceanic and Atmospheric Administration (NOAA Center for Tsunami Research, <http://nctr.pmel.noaa.gov/tsunami-forecast.html>), and pre-computed inundations of a fixed bell-shaped waveform are used in Chen et al. (2014).

The Carrier-Greenspan transformation derived by Carrier and Greenspan (1958) is a classic exact solution for the 1-D coupled fully nonlinear shallow water equations over a uniform slope and is applied to evaluate the tsunami induced runup height and its inundation distance in this present study. This solution is difficult to transform in terms of the real space and time domain. The semi-analytical solution, a more convenient form associated with an analytical Green's function (AGF) related to the total mechanical energy, is developed by Carrier, Wu and Yeh (2003). It is called CWY algorithm. The total mechanics energy can be integrated for any initial conditions by using common integration software, such as IMSL of Fortran. Then, the temporal and spatial variation of tsunami induced runup height, flow velocity, inundation distance and momentum flux on coastal areas can be determined.

The CWY algorithm was used to estimate the tsunami runup height for numerous real tsunami events by Chen et al. (2012). More recently, this algorithm has been put forward to predict tsunami runup height more quickly when linked with an existing database based on the reciprocal Green's function (see also Chen et al., 2014). Hereinafter it is called the RGF database. In their process, an initial condition taking 3~5 representative waves from the wave data is applied in CWY algorithm. The speed of numerical integration depends on the length of representative waves. Determining the reasonable representative waves and excessive computing times are the problems in their studies.

¹ International Wave Dynamics Research Center (IWDRC), Tainan Hydraulics Laboratory-National Cheng-Kung University, No.500, Sec.3, Anming Rd., Tainan, Tainan, 70955, Taiwan, R.O.C

² Department of Oceanography, National Sun Yat-Sen University, No.70, Lienhai Rd, Kaohsiung, Kaohsiung, 80424, Taiwan, R.O.C

In order to enhance the computing efficiency, conveniently build the database and avoid the uncertainty in choosing the representative waves, modifications are proposed in the present study. The basic concept is that the principle of superposition is applied to calculate the total mechanics energy, replacing the complicated numerical integration in CWY algorithm. Because of the numerous individual energy-components decomposed from the incident waveform are pre-integrated beforehand and saved as a database, this improvement can save a lot of computing time. The establishment of a runup database is described in Sec. 2. In Sec. 3, we will introduce the applications on real tsunami events, and the present results reasonably coincide with the in-situ surveys. Finally, the forecasted accuracy, the computing efficiency and the integration with RGF database are discussed in the last chapter.

2. Methodology

2.1 1D Carrier-Wu-Yeh algorithm and analytical Green's function

CWY algorithm is the 1D semi-analytical solution, and an idealized approach with neglecting the breaking wave, the turbulence and the influence of a boundary layer. The derivation is briefly displayed in this section and the details can be found in the published papers, such as Carrier et al. (2003) and Chen et al. (2012).

As depicted in Fig.1, the fully nonlinear shallow water wave equations for propagation over a uniform mild constant slope α can be written as

$$\begin{aligned} [u(x+\eta)]_x + \eta_t &= 0, \\ u_t + uu_x + \eta_x &= 0. \end{aligned} \quad (1)$$

The x -coordinate points is in the offshore direction from the shoreline. In the eq.(1), the following scaling parameters are employed:

$$u' = u / \sqrt{g\alpha L}, \quad \eta' = \eta / \alpha L, \quad x' = x / L, \quad t' = t \sqrt{\alpha g / L}, \quad (2)$$

It notes that a primed superscript represents the dimensionless physical quantities. L is an arbitrary convenient horizontal characteristic length, u' is the horizontal flow velocity, η' is the wave elevation, g is the gravitational acceleration, x' and t' are the horizontal coordinate and time, respectively. Eq.(1) can be expressed in the nondimensional form,

$$\begin{aligned} [u'(x'+\eta')]_{x'} + \eta'_{t'} &= 0, \\ u'_{t'} + u'u'_{x'} + \eta'_{x'} &= 0. \end{aligned} \quad (3)$$

The beach slope α and the gravity acceleration g no longer exist in the shallow water wave equation.

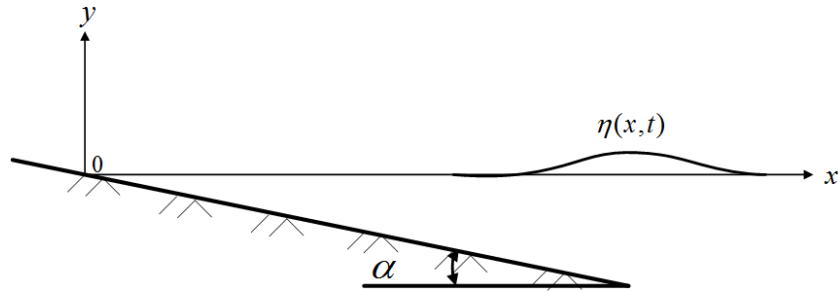


Fig.1 Tsunami waves over the beach with uniform slope.

Introducing the distorted coordinate system (σ, λ) ,

$$\lambda = t' - u', \quad \sigma = \sqrt{q} = \sqrt{x' + \eta'}, \quad (4)$$

where q is the inundation distance and $\sigma = 0$ is the moving shoreline. The parameter ψ and the new

function ϕ are related to the total mechanical energy $\eta' + \frac{1}{2}u'^2$ by the relation

$$\psi = \eta' + \frac{1}{2}u'^2 = \phi_\lambda. \quad (5)$$

The unknown flow velocity u' and wave elevation η' can be determined by the function ϕ as:

$$u' = -\frac{\varphi_\sigma}{2\sigma}, \quad \eta = \varphi_\lambda - \frac{\varphi_\sigma^2}{8\sigma^2}. \quad (6)$$

Then, eq.(3) can be reduced to a linear cylindrical-wave equation by using the nonlinear transformation (Bernard and Robinson, 2009),

$$4\sigma\varphi_{\lambda\lambda} - (\sigma\varphi_\sigma)_\sigma = 0. \quad (7)$$

The general solution of eq.(7) with integral form can be solved by using general initial conditions and the Fourier-Bessel transform,

$$\varphi(\sigma, \lambda) = 2\left\{\int_0^\infty F(b)G(b, \sigma, \lambda)db + \int_0^\infty P(b)G_\lambda(b, \sigma, \lambda)db\right\}. \quad (8)$$

Two independent initial conditions at $\lambda=0$ are The spatial offshore waveform $F(b)$ and flow velocity $P(b)$, respectively. b is the spatial dummy variable in the distorted coordinate. Eq. (8) shows that the function $\varphi(\sigma, \lambda)$ comprises both the potential and kinematic components. $G(b, \sigma, \lambda)$ is called the Analytical Green's Function (AGF) (Chen et al., 2012) and can be explicitly expressed as

$$G(b, \sigma, \lambda) = \begin{cases} 0 & \text{for } \frac{1}{2}\lambda < |\sigma - b| \\ \frac{1}{\pi} \sqrt{\frac{b}{\sigma}} K\left(\frac{\lambda^2 - 4(\sigma - b)^2}{16\sigma b}\right) & \text{for } |\sigma - b| < \frac{1}{2}\lambda < |\sigma + b|. \\ \frac{4}{\pi} \frac{b}{\sqrt{\lambda^2 - 4(\sigma - b)^2}} K\left(\frac{16\sigma b}{\lambda^2 - 4(\sigma - b)^2}\right) & \text{for } \frac{1}{2}\lambda > |\sigma + b| \end{cases} \quad (9)$$

$K(k) = \int_0^{\pi/2} \frac{d\theta}{\sqrt{1 - k \sin^2 \theta}}$ is a first kind complete elliptic function.

The advantages of CWY algorithm are that it can obtain quite accurate results for an arbitrarily selected temporal/spatial domain without computing other domains and conveniently inverse to presentations in the real physical coordinate. It also serves as a benchmark and can verify the modeled results in the prediction of shoreline movements and runup (Carrier et al., 2003).

In fact, the magnitude of the initial velocity $P(b)$ is much smaller than that of wave elevation according to the characteristics of initial seafloor deformation and tsunami simulation (Carrier et al., 2003; Chen et al., 2012). Hence, in eq.(8), the second term can be neglected and is approximated as

$$\varphi(\sigma, \lambda) \approx 2\int_0^\infty F(b)G(b, \sigma, \lambda)db. \quad (10)$$

This notes that the potential energy induced by $F(b)$ is the dominant component. $F(b)$ is the spatial waveform normal to the shoreline, however, only temporal data can be received from tide sections or GPS buoys. Chen et al. (2012) suggest an equivalent spatial waveform transformed from the original time series as a representative initial/boundary condition and the mathematical transformations are shown as follows,

$$\bar{x} = \frac{1}{4} s \bar{t}^2 g + \bar{t} \sqrt{g d_0} + \frac{d_0}{s}, \quad \eta_e = \eta_0 \sqrt[4]{\frac{d_0}{s x}}, \quad \bar{x} = b^2. \quad (11)$$

In eq.(11), \bar{t} is time in sec, \bar{x} is the spatial coordinate corresponding to the elapsed time, $s = \tan \alpha$ is the bottom slope, and d_0 is the local water depth at the boundary point. η_0 and η_e are the wave elevation of original temporal records and equivalent spatial waveform, respectively. For arbitrary random tsunami waves, the equivalent waveform $F(b)$ in the linear region (deeper than 50 m) can be decomposed by FFT and $\varphi(\sigma, \lambda)$ can be integrated by IMSL further. Thus, the dimensional runup height and inundation distance can be estimated via eq.(5).

2.2 Pre-calculated dataset

Recall the Fig.1, the point R_i is called the offshore boundary point corresponding the forecast point P_i on the land. The characteristic length L_i , the local water depth d_0 and the slope can be determined by the digital terrain model. Therefore, the arbitrary spatial waveform $F_i(b)$ can be obtained by applying the eq.(10) after receiving the temporal data of offshore boundary point R_i .

An arbitrary spatial waveform $F_i(b)$ at a boundary point R_i can be decomposed by Fourier series

$$F_i(b) = \bar{\eta} + \sum_{j=1}^n A_j \cos(\omega_j b) + \sum_{j=1}^n B_j \sin(\omega_j b). \quad (12)$$

Substituting eq.(12) into eq. (10), function φ can be expressed as the following matrix form (Lin et al., 2014),

$$\varphi(\sigma, \lambda) = \begin{bmatrix} \bar{\eta} & \sum_{j=1}^n A_j & \sum_{j=1}^n B_j \end{bmatrix} \begin{bmatrix} D_0 \\ D_{cj} \\ D_{sj} \end{bmatrix}. \quad (13)$$

n is the number of Fourier components, and $\begin{bmatrix} D_0 & D_{cj} & D_{sj} \end{bmatrix}$ can be shown to be

$$D_0 = 2 \int_0^\infty G(b, \sigma, \lambda) db, \quad (14)$$

$$D_{cj} = 2 \int_0^\infty \cos(\omega_j b) G(b, \sigma, \lambda) db, \quad (15)$$

$$D_{sj} = 2 \int_0^\infty \sin(\omega_j b) G(b, \sigma, \lambda) db. \quad (16)$$

Where $\bar{\eta}$, A_j , B_j and ω_j are Fourier coefficients of $F(b)$ determined by Fast Fourier Transformation (FFT). D_0 is the constant component. D_{cj} and D_{sj} related to ω_j are components of j-th cosine and sine waves, respectively. It should be noted that D_0 , D_{cj} and D_{sj} all are independent of the mean level $\bar{\eta}$, wave amplitudes A_j and B_j . Eqs. (14)~(16) can be integrated beforehand for various ω_j in the domain (σ, λ) and saved as a database. The equivalence of eqs. (10) and (13) indicates that the function $\varphi(\sigma, \lambda)$ can be determined by using simple superposition and multiplication rather than direct integration, thus allowing computing time to be saved.

2.3 Verification for the equivalency of eqs.(9) and (12)

In this section, a simulated wave data modeled by COMCOT at Patong beach ($98.2^\circ E, 7.9^\circ N$) in the western Phuket area in 2004 Indian tsunami event is used to verify the equivalency of eqs.(9) and (12), and carefully discuss the calculating error. The fault parameters are listed in next section. The boundary point is 8.64 km away from the shoreline and its slope of bottom α is 0.039 based on the local bathymetry received from ETOPO2.

The simulated wave time series of boundary point $F(t)$ is 3hours and its sampling frequency is 0.016Hz. Its equivalent waveform is determined by eq.(11) and its Fourier spectrum with 90 components are illustrated in Fig.2(a)(b)(c), respectively. Using the FFT, the Fourier coefficients can be obtained. Hence, the explicit waveform can be determined and the total mechanical energy also can be calculated using eq.(10). On the other hand, the corresponding components D_0 , D_{cj} and D_{sj} can be found from the pre-setting runup database. Therefore, the total mechanical energy also can be calculated by using eq.(13). The total mechanics energy are plotted in Fig.3(a). Their error is displayed in Fig.3(b). The small errors proof that eq.(10) and eq.(13) are equivalent. Fig.3(c) shows that the spatial/temporal variation of wave displacement including incident/outgoing waves and the moving shoreline in the nondimensional time/space domain. Thus, the dimensional runup height and the inundation distance can be inversely determined by using eq.(2). The variation of wave displacements and the moving shoreline on the coastal region with $-0.2 \leq x \leq 0.2$ and $0 \leq t \leq 15$ is shown in Fig.3(d).

The detailed error analysis indicates that the maximum error is occurred in $\sigma = 13$ and $\lambda = 16$, as shown in Fig.4. This is because the calculating errors are cumulated at the boundaries. However, the total mechanical energy and the forecasted results are not significantly influence by small errors. Based on the numerical testing for computing efficiency, the computing time using the two equations are respectively 52 min and 2 sec for the same-length time series, the computing domain ($\sigma = 13, \lambda = 16$) and the same desktop

PC having a Microsoft Windows 7 operating system with 4GB RAM and an Intel Core i7-3770 with two 3.40GHz CPU. The result implies that the present approach can save a lot of computing time.

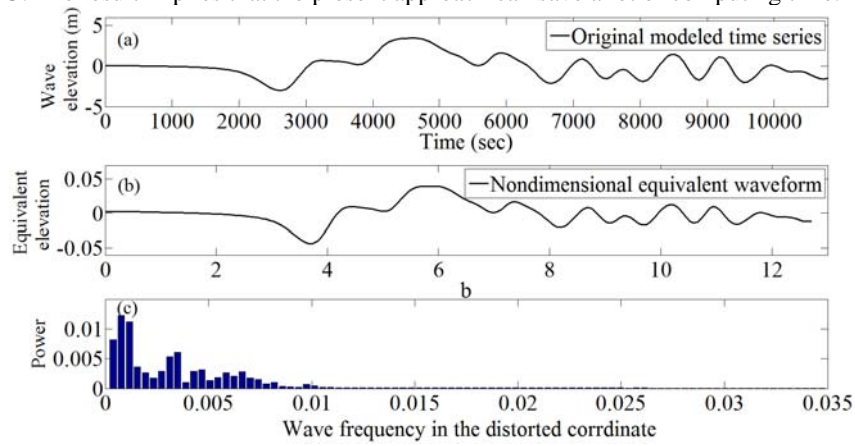


Fig.2 (a) Numerical three-hour waveform time series with sampling frequency 0.016Hz, (b) the spatially equivalent waveform at $(98.2^{\circ} E, 7.9^{\circ} N)$ on Patong beach and (c) the Fourier spectrum with 90 components.

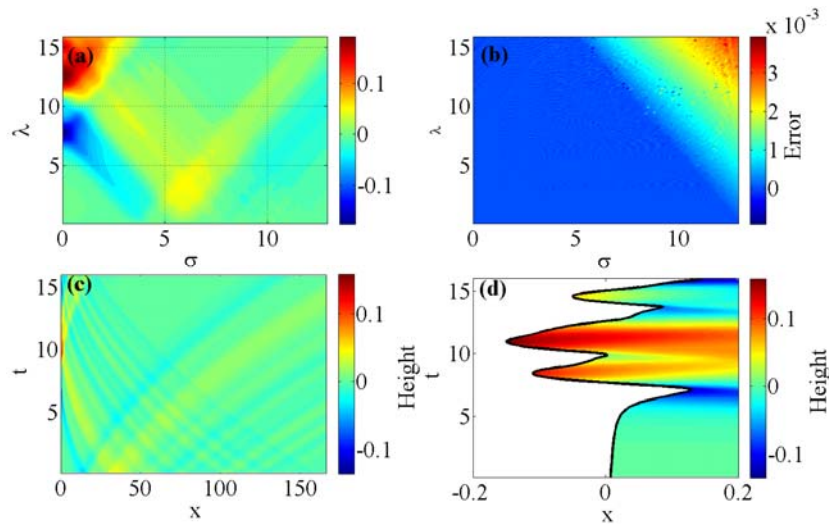


Fig.3 (a) The total mechanics energy $\varphi(\sigma, \lambda)$ calculated by eq.(13), (b) the error distribution between eq.(10) and eq.(13), (c) the spatial and temporal variation of wave displacement in the physical domain (x, t) and (d) the variation of the wave displacement and the moving shoreline on the coastal region.

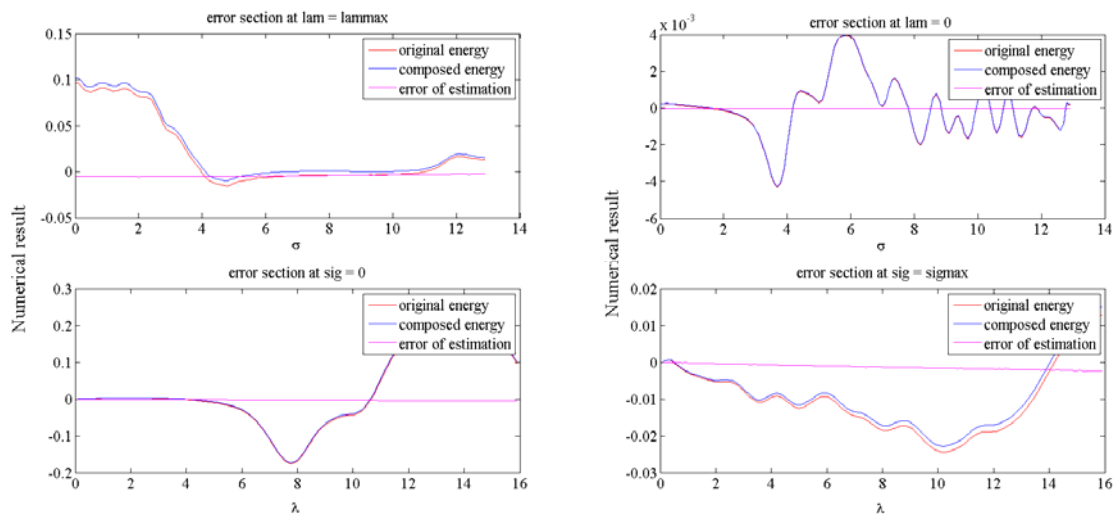


Fig.4 The errors are at the boundaries of computing domain.

3 Application to real tsunami events

3.1 2004 Indian tsunami

In this section, two real cases in 2004 Indian tsunami, Phuket Island and East Sri-Lanka, are applied to verify the present methodology. The submarine earthquake induced Indian Ocean Tsunami with a moment scale magnitude (M_w) 9.1 occurred offshore of Banda Aceh ($95.982^\circ E, 3.295^\circ N$), Indonesia at 00:58:53 UTC on December 26, 2004. The focal depth was 30km. Approximately 227,000 people died in this tsunami event based on the published information. More detailed information can be found in the National Geophysical Data Center (NGDC) of the NOAA (<http://www.ngdc.noaa.gov/hazard/tsu.shtml>).

Phuket Island and East-Lanka are located at the eastern and western sides of tsunami source, respectively. Phuket 500 km east of the epicenter is a famous resort area in southern Thailand. In the 2004 Indian Ocean Tsunami, the death toll was approximately 5,400 persons. The western coast of Phuket is called the KhaoLak coast (Latitude $7.8 \sim 8.7^\circ N$). The tsunami waves hit Phuket Island and the KhaoLak coast about two hours after the earthquake (Murata et al., 2011). The runup heights of 3.9~9.8m in the zone have been recorded in the field investigation. On the other hand, east Sri-Lanka is 1500 km away to the west of the epicenter. The 700~800km/h speed of the leading tsunami wave with wave height 1 m hit the region 2 hours after the earthquake. The fundamental period was approximately 40~50 minutes, and its wavelength was more than 100 km. The tsunami height was 5~10m on the eastern coast, and 4~10m in the southern region (Murata et al., 2012). Based on the report of Wijetunge (2006), the number of refugees created by the tsunami was 78,000, and more than 41,000 people died on this island.

In this simulation, the fault parameters suggested by Tomita et al.(2005) are employed, as shown in Table1. The initial waveform in the source area is also plotted in Fig.5. In the case of Phuket Island, determining the offshore boundary points and the corresponding forecasted points on the land based on ETOPO2 2min gridded data is the first step. Thus, the characteristic lengths and the slopes can be determined, as listed in Table 2. In this form, it is found that the local water depths of these offshore boundary points are approximately 50m. The offshore distances in the Phuket coast are slightly longer than that in the East Sri-Lanka. This is because there are the longer mild slopes in the Phuket's offshore regions. The distribution of points and their simulated time series with the sampling frequency 0.016 Hz are plotted in Fig.6(a)(b), respectively. Based on the present process, the forecasted results can be shown in Fig.7. The 5.67~10.68m forecasted runup heights quite approach the measured runup height 3.9~9.8m. Even if the forecasted result at Bang-Thao beach is overestimated by 4 times, the forecasted accuracy is reasonable and reliable.

Table 1 The fault parameters for the 2004 Indian Ocean Tsunami.

Source parameters	Segment 1	Segment 2	Segment 3
Epicenter depth(km)		5	
Dislocation (m)		15	
Fault width(km)		150	
Fault length(km)	200	670	300
Strike/Dip/Slip	300/13/90	345/13/90	365/13/90

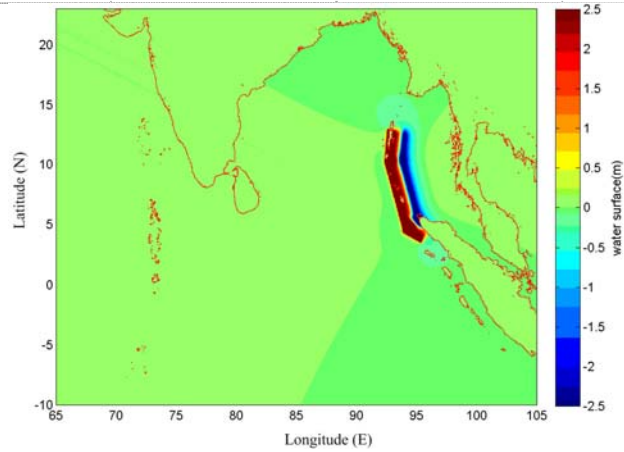


Fig.5 The initial free surface elevation of 2004 Indian Ocean Tsunami based on Tomita et al. (2005)

Table 2 The locations of forecast points and boundary points for Phuket coast.

Location	Forecast points (N, E)	Boundary points (N, E)	Local water depth (m)	Slope α	Offshore distance L (km)
Phuket coast					
Kata Noi beach	7.8, 98.28	7.8, 98	67	0.0022	30.24
Patong beach	7.9, 98.28	7.9, 98.2	34	0.0039	8.64
Bang Thao beach	8, 98.29	8, 98.2	37	0.0038	9.72
Khao Lak beach	8.2, 98.30	8.2, 98.07	49	0.002	24.84
Bah Kao Lak	8.6, 98.23	8.6, 98.13	46	0.0043	10.8
Nan Niang beach	8.7, 98.23	8.7, 98.13	49	0.0045	10.8
East Sri-Lanka					
Potuvil(1)	6.8, 81.8	6.8, 82	50	0.0023	21.6
Potuvil(2)	7, 81.87	7, 81.93	34	0.0052	6.48
Akkaraioattu	7.2, 81.85	7.2, 81.9	50	0.0093	5.4
Kalmunai(1)	7.4, 81.83	7.4, 81.93	50	0.0046	10.8
Kalmunai(2)	7.6, 81.77	7.6, 81.867	48	0.0045	10.584
Batticala	7.8, 81.61	7.8, 81.667	51	0.0084	6.048
Kalkudah	8, 81.476	8, 81.6	98	0.0073	13.392

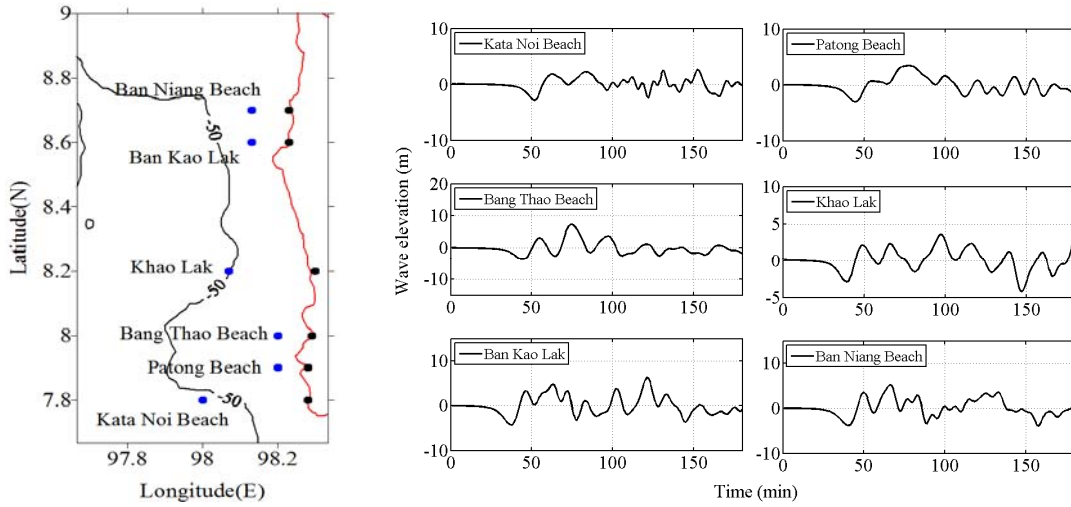


Fig.6 The distribution of offshore boundary points and their simulated time series with the sampling frequency 0.016 Hz on Phuket coast.

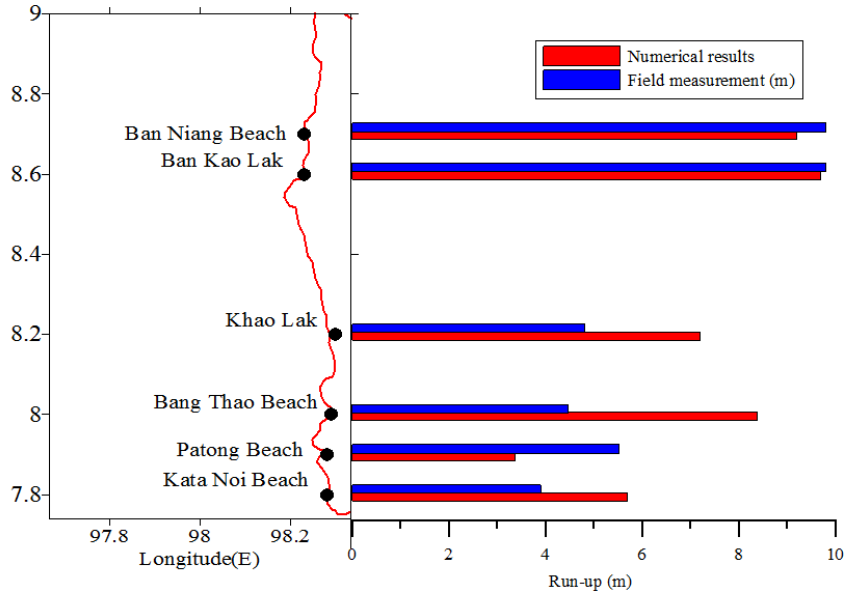


Fig.7 The comparison between the present results and filed measurement on the Phuket coast.

In the case of East Sri-Lanka, seven offshore boundary points and corresponding land-points are set along the eastern coast and the corresponding numerical wave time series are depicted in Fig.8, respectively. Their locations and topographical parameters are found in Table.3 The coastal line in East Sri-Lanka is straight without any particular geomorphologies , and more regular than that in Phuket coast. Fig.9. displays the comparison between forecasted and in-situ results. the 579~2117m estimated inundation distances are close to the field investigation. The estimated maximum runup heights 4.9m~8.1m are agreement to the in-situ survey. The runup heights are slightly underestimated at latitudes $6.8^{\circ}N$ and $8^{\circ}N$.

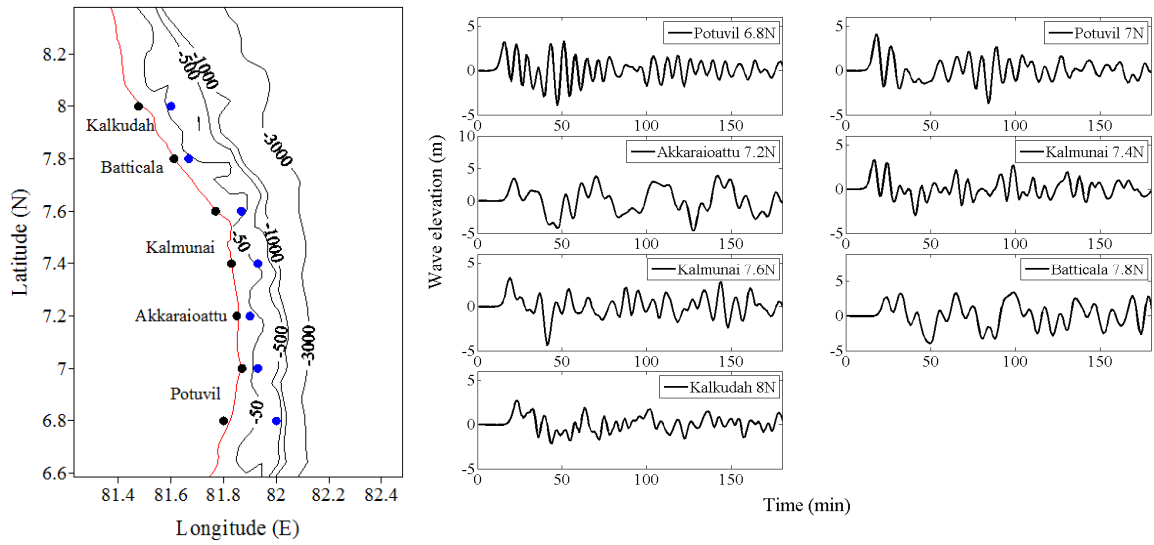


Fig.8 The distribution of offshore boundary points and their simulated time series with the sampling frequency 0.016 Hz on east coast of Sri-Lanka.

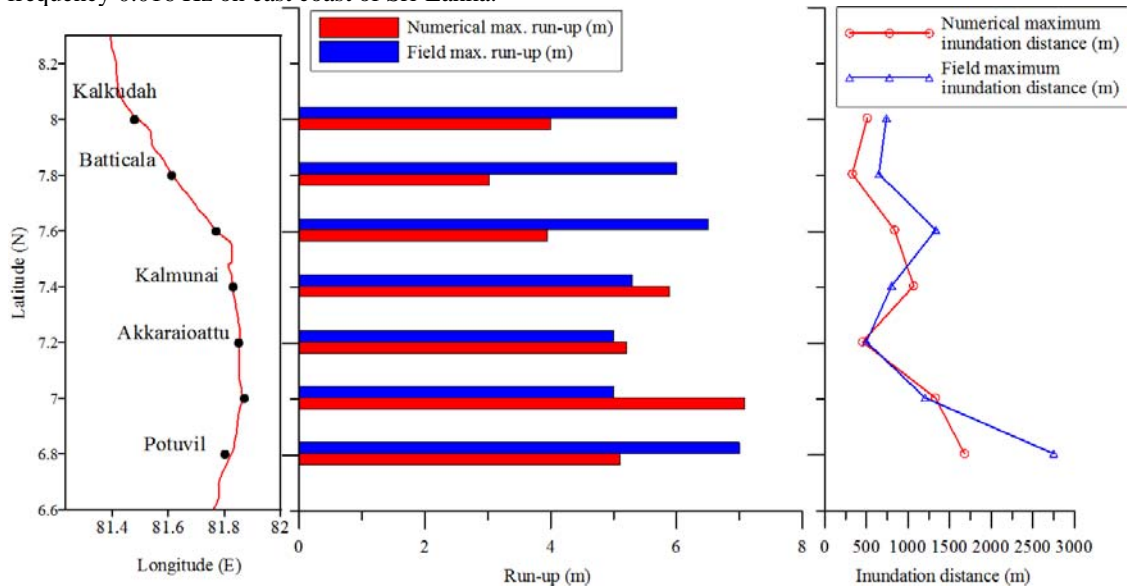


Fig.9 The comparison between the present runup height/inundation distance and filed measurement in the East Sri-Lanka.

3.2 2011 Tohoku tsunami

At 14:46:23 local time (5:46:23 UTC) on March 11, 2011, a strong submarine earthquake with scale magnitude 9.0 occurred offshore at ($142.842^{\circ} E$, $38.297^{\circ} N$) in the northeast of Japan. The rupture area was conjectured to be approximately $450\text{km} \times 200\text{km}$ (Mori et al, 2011) and the focal depth is 29m. The tsunami leading waves arrived at the Tohoku district (including Aomori/Iwate/Miyagi/Fukushima Prefectures) 20 min after the earthquake. The huge tsunami hit over the whole Tohoku region including in Sendai, the largest city, and on the Sendai Plain, which is the most populous area in this district (Mori et al., 2012). Ultimately, tsunami waves hit the whole of Japan's Pacific coast 2000 km in length (Mori et al., 2011). The Japan Meteorology Agency (JMA, 2011) issued the first tsunami warning 3 minutes (14:49 local time) after the earthquake where the forecasted runup height was 3m in Iwate, 6m in Miyagi and 3m in Fukushima. Later, the forecasted runup heights all were upgraded to over 10m. Based on the disaster survey reported on the NOAA-NGDC website, it caused a death toll of approximately 18,000 and 210 billion U.S. dollars damage. The investigation showed that the maximum runup height of 40m was at Ofunato (Latitude

38 ~ 40° N), and 19.5m maximum inundation depth and over 4km of inundation distance were in the Sendai bay (Mori et al., 2012; Goto et al., 2012; Sugawara et al., 2013). This tsunami event caused severe damage to regions along the Pacific coast of Japan.

The in-situ data in Iwate, Miyagi and Fukushima Prefectures are applied to verify the present approach. It is different from the first two cases that the temporal wave records measured by the GPS buoys (No. 807, 804, 802, 803, 801 and 806) of NOWPHAS (Nationwide Ocean Wave information network for Ports and Harbours, website: http://nowphas.mlit.go.jp/news_chn.html) are used as the initial condition for offshore boundary points. These GPS buoys are deployed in the offshore region with 125m~204m water depth and 14~60km offshore distance. The detailed information and the 5h time series (14:46:20~19:46:20 local time) with 0.2Hz sampling frequency recorded by GPS buoys are shown in Table 3 and Fig.10, respectively.

The present results for the maximum runup height are plotted in Fig.11. The estimated runup heights are 5.4~10.6m in north/central/south Iwate, 8.3~10.5m in north/central Miyagi and 4.75m in Fukushima. The results agree with the preliminary predictions of the JMA and the field measurement afterwards. The predictions in particular locations, such as north/central Iwate and north Miyagi, are found to underestimate approximately 1/3~1/2. The typical reasons and the present accuracy are discussed in next section.

Table 7 The locations of GPS buoys and topographical parameters.

No./Section	Local water depth(m)	Position (N, E)	Slope α	Offshore distance L (km)
807 North-Iwate	125	40°07'00" , 142°04'00"	0.0063	19.88
804 Central-Iwate	200	39°37'38" , 142°11'12"	0.0142	14.04
802 South-Iwate	204	39°15'31" , 142°05'49"	0.012	16.95
803 North-Miyagi	160	38°51'28" , 141°53'40"	0.00836	19.13
801 Central-Miyagi	144	38°13'57" , 141°41'01"	0.00243	59.27
806 Fukushima	137	36°58'17" , 141°11'08"	0.007	19.37

NOWPHAS website: http://nowphas.mlit.go.jp/news_chn.html

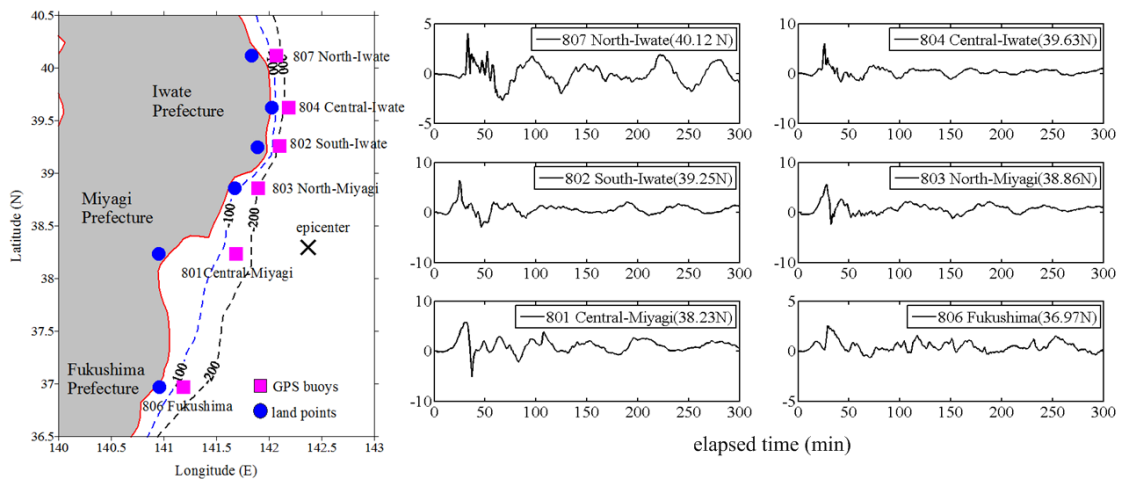


Fig.10 The locations of GPS buoys and the 5h time series (14:46:20~19:46:20 local time) with 0.2Hz sampling frequency.

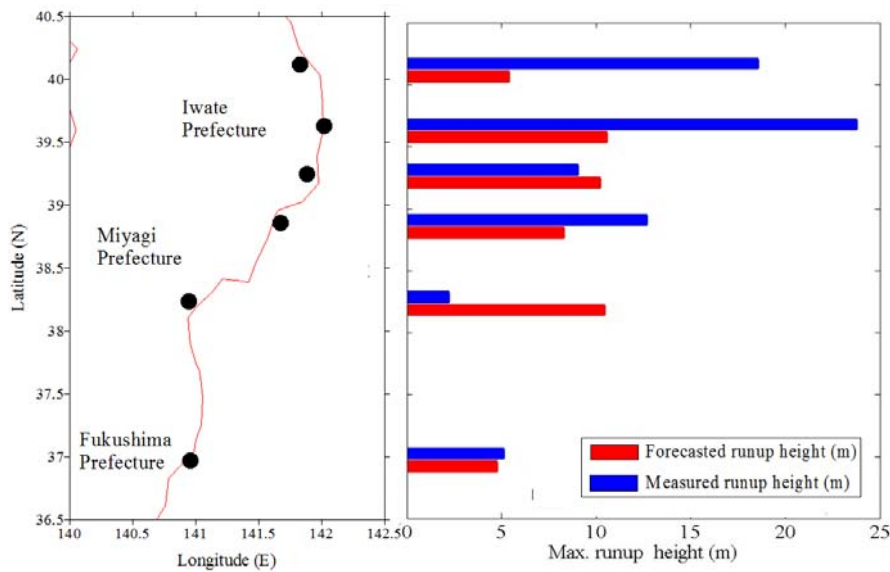


Fig.11 The comparison between the present results and filed measurement on Tohoku coast.

4 · Discussion

4.1 Forecast accuracy

The present accuracy is discussed in this section. The present methodology can provide the reasonable runup height and an order-of-magnitude-accuracy the inundation distance. The forecasted deviations with the maximum runup height for total 19 testing points (3 cases) are illustrated in Fig.12. The larger forecasted deviations occur in the Tohoku case. This is because there are many quite irregular and consists of bays, tips of capes, coves and narrow embayments along Tohoku's coastal line. The tsunami energy is concentrated in these regions and can cause the wave reflection, refraction and interactions effects, such as resonance, between bays and tsunami waves. These factors can cause extreme runup heights in comparison with the surrounding area (Murata et al., 2012; Yim et al., 2012). Therefore, most results display that estimated runup heights are conservatively overestimated, and that in the Tohoku regions are not.

In this present algorithm, ETOPO2 is used to determine the slope of bottom. However, the tsunami is a very long wave so that its behavior is not sensitive to small scale bathymetric features. Hence, ETOPO2 can provide satisfactory bathymetry for tsunami runup. On the other hand, the determination of inundation distance depended on the potential energy and the slope of the sea bottom. The slope of the sea bottom in the coastal region is usually different from that of the land (Chen et al., 2012). Real inundation areas are related to the realistic landform, the arrangement of surface features and geomorphic factors. Although these influences of bathymetry are not fully considered in this approach, the predications are still reasonable based on the comparisons shown in the previous section.

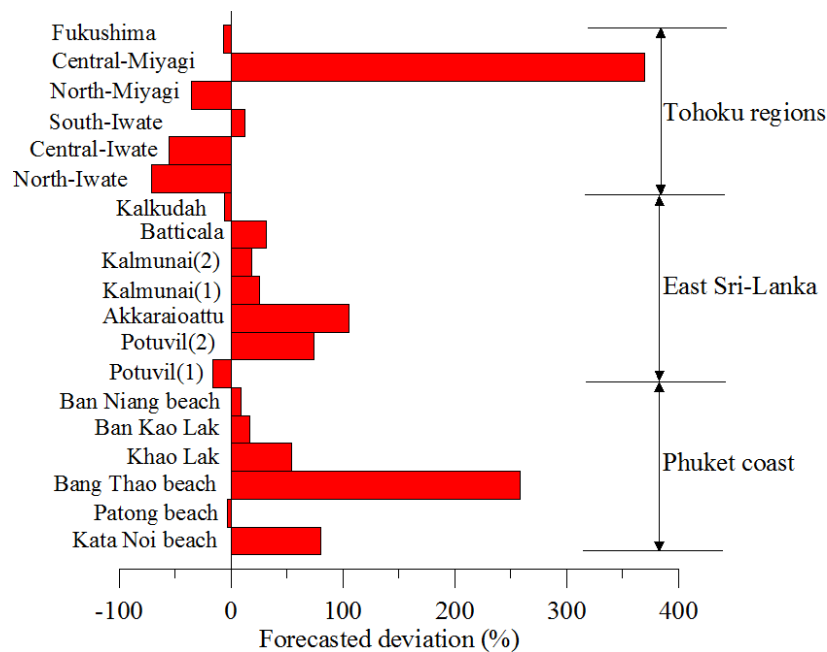


Fig.12 The forecasted deviation for 19 testing points with three regions.

4.2 Computing efficiency

The computing efficiency of eq.(10) and eq.(13) are discussed in this section. Chen et al.(2012) estimated the runup heights and inundation distances in the East Sri-Lanka and Phuket by directly integrating eq.(10). Eq.(13) is used to calculate the function $\varphi(\sigma, \lambda)$ for the same regions in the present study. It is noted that the computing time is proportional to the Fourier components in the direct integration. The computed time using the present approach is approximately 20 sec for the 7 points in East Sri-Lanka, 10 sec for the 6 points in the Phuket and 15 sec for the 6 points in the Tohoku region, depending on the computing domain. Hence, the efficiency of the present pre-calculated data base is much better than that of the direct integration. Thus, the present approach can significantly enhance the computational efficiency in disaster early assessment. A complete tsunami early warning integrating with an existing RGF database for a particular city that would include offshore wave elevation, runup height and inundation distance on the coastal region could be issued within a few minutes.

4.3 Combination with the local early tsunami warning system for Taiwan's coastal regions

Chen et al.(2012) developed the local tsunami warning system for Taiwan's coastal regions based on the reciprocal Green's function (RGF), as shown in Fig.13. In this system, it can quickly provide the initial waveform of the tsunami in source area, the wave time series of boundary points and the corresponding regional inundation map for a certain location after automatically receiving the fault parameter from the particular website, such as USGS (Chen et al., 2014). Numerous offshore numerical points already are arranged the linear regions (deeper than 50 m) and applied to provide the wave time series data after the tsunami occurred. Hence, these points can be used to set as offshore boundary points in the present study.

Integrating the RGF database and the present methodology is the further work in the future. A numerical record taken from the RGF database is suggested to be an initial/boundary condition in the present algorithm because it can be determined by the local RGF database in a few minutes. This is a more convenient way in comparison to those of 2D direct tsunami simulation and the single point in-situ measurement (such as offshore buoys/sensors/tidal sections) (Lin et al., 2014). Then, the maximum runup height and its inundation distance for a certain location will be evaluated by the above-mentioned process. It is going to provide more useful information for the prevention and mitigation of tsunami disaster on coastal regions.

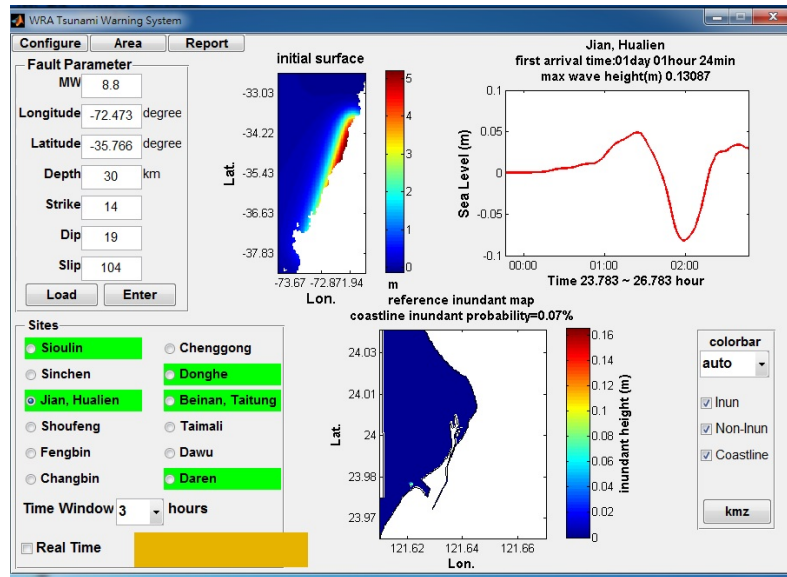


Fig.13 The user interface of local tsunami warning system for Taiwan's coastal regions.

Acknowledgements

This paper was completed with grants from the Ministry of Science and Technology–International Wave Dynamics Research Center (NSC 103-2911-I-006-302) and the Center of Harbor and Marine Technology (MOTC-IOT-102-H3DB001b) of Taiwan, Republic of China. The authors also thank the Japan Meteorology Agency (JMA) for providing the in-situ data for GPS buoys.

Reference

- Bernard, E. D. and A. R. Robinson. 2009. *Tsunamis*, Harvard University, USA.
- Carrier, G. F. and H. P. Greenspan. 1958. Water waves of finite amplitude on a sloping beach, *J. Fluid Mech.*, 4, 97-109.
- Carrier, G. F., T. T. Wu and H. Yeh. 2003. Tsunami runup and drawdown on a plane beach, *J. Fluid Mech.*, 475, 79–99.
- Chen, G. Y., C. H. Lin and C. C. Liu. 2012. Quick evaluation of runup height and inundation area for early warning of tsunami, *Journal of Earthquake and Tsunami*, 6(1), 1250005-1–1250005-2.
- Chen, G. Y., C. C. Liu and C. C. Yao. 2014. A Forecast System for Offshore Water Surface Elevation With Inundation Map Integrated for Tsunami Early Warning, *IEEE Journal of Oceanic Engineering*, doi: 10.1109/JOE.2013.2295948.
- Goto, K., K. Fujima, D. Sugawara, S. Fujino, K. Imai, R. Tsudaka, T. Abe and T. Haraguchi. 2012. Field measurement and numerical modeling for the run-up heights and inundation distance of the 2011 Tohoku-oki tsunami at Sendai Plain, Japan, *Earth Planets Space*, 64, 1247–1257.
- Japan Meteorological Agency. 2011. Report of natural phenomenon in Heisei 23 years of disasters (In Japanese), Japan Meteorological Agency.
- Lin, J. H., Y.F.Chen, C. C. Liu and G. Y. Chen. 2014. Building a pre-calculated quick forecast system for tsunami run-Up height, *Journal of Earthquake and Tsunami*, 8(3), 1440002-1-1440002-24.
- Mori, N., T. Takahashi, T. Yusuda and H. Yanagisawa. 2011. Survey of 2011 Tohoku earthquake tsunami inundation and run-up, *Geophysical Research Letters*, 38, L00G14.
- Mori, N., T. Takahashi and The 2011 Tohoku Earthquake Tsunami Joint Survey Group. 2012. Nationwide post event survey and analysis of the 2011 Tohoku earthquake tsunami, *Coastal Engineering Journal*, 54(1), 1250001-1–1250001-27.
- Murata, S., F. Imamura, K. Katoh, Y. Kawata, S. Takahashi and T. Takayama. 2011. *Tsunami: to survive from tsunami*, World Scientific, Singapore.
- Sugawara, D., F. Imamura, K. Goto, H. Matsumoto and K. Minoura. 2013. The 2011 Tohoku-oki earthquake tsunami: similarities and differences to the 869 Jogan tsunami on the Sendai plain, *Pure Appl. Geophys.*, 170, 831–843.

Tomita, T. et al. [2005] Numerical Simulation of the 2004 Indian Ocean Tsunamis (in Japanese), Report of Port and Airport Research Institute. USGS Web site, <http://earthquake.usgs.gov/eqcenter/eqinthenews/2004>.

Yim, S. C, K. F. Cheung, M. J. Olsen and Y. Yamazaki. 2012. Tohoku tsunami survey, modeling and probabilistic load estimation applications, *Proceedings of the International Symposium on Engineering Lessons Learned from the 2011 Great East Japan Earthquake*, Tokyo, Japan.

NGDC http://www.ngdc.noaa.gov/hazard/honshu_11mar2011.shtml.

NOWPHAS http://nowphas.mlit.go.jp/news_chn.html.